Composites Part B 102 (2016) 1–8

Contents lists available at ScienceDirect

Composites Part B

journal homepage: www.elsevier.com/locate/compositesb

Pullout strength of graphene and carbon nanotube/epoxy composites

Y. Chandra [a], F. Scarpa [b], S. Adhikari [a, *], J. Zhang [c], E.I. Saavedra Flores [d], Hua-Xin Peng [e]

[a] Zienkiewicz Centre for Computational Engineering, Swansea University, Swansea, SA1 8EN, UK
[b] Advanced Composites Centre for Innovation and Science, University of Bristol, Bristol, BS8 1TR, UK
[c] Department of Material Science and Engineering, National University of Defence Technology, Changsha, Hunan, 410073, PR China
[d] Departamento de Ingeniería en Obras Civiles, Universidad de Santiago de Chile, Av. Ecuador 3659, Santiago, Chile
[e] Institute for Composites Science Innovation, School of Materials Science and Engineering, Zhejiang University, Hangzhou, 310027, PR China

ARTICLE INFO

Article history:
Received 18 October 2015
Received in revised form
3 May 2016
Accepted 16 June 2016
Available online 7 July 2016

Keywords:
Graphene sheets
Carbon nanotubes
Nanocomposites
Finite element
Shear strength

ABSTRACT

An atomistic multiscale modelling approach is used to simulate the nonlinear pullout behaviour of interlinked single walled carbon nano tubes (SWCNT) and single layer graphene sheets (SLGS) embedded in an epoxy polymer. The pullout forces have been computed for various configurations of nanocomposites (SWCNT-SWCNT, SLGS-SLGS and hybrid SLGS-SWCNT), also by evaluating the effect provided by three different interlink compounds. The interfacial strength due to fibre pullout predicted by the hybrid atomistic-FE model is compared against experimental and molecular dynamics results available in open literature. The results show the specific deformation characteristics (localised auxetics) that provide an increase of pullout forces and interfacial strength with the use of the links.

1. Introduction

Carbon based nanomaterials such as graphene sheets and CNTs display exceptional mechanical [1–10] and electrical [11–16] properties. These nanostructures can be used to reinforce polymers and in general multifunctional composites and devices [17–24]. Graphene sheets can be mechanically exfoliated from graphite, chemically modified and then be embedded in polymer solution [25], or dispersed in an organic solution and then used as stable fillers in polymers [26]. CNT reinforced polymer composites can be produced by casting in a polymer [27], or typically by dispersing CNTs in a solvent by sonication followed by mix in a polymer liquid with ensuing evaporation of the initial solvent [28].The demand for nanocomposites in industrial applications is ramping up [29], however some drawbacks are still present in the modern production of carbon-based structural materials. More specifically, some of the main problems are represented by an inadequate bonding between the matrix and reinforcement, the difficulty of producing a uniform dispersion within the matrix, and in general the generation of homogeneous dispersions in large-scale composite structures. However, the molecular bridging between nano structures within the polymer can enhance the structural performance of the composite [30] and overcome the drawback represented by the inadequate bonding strength.

To reduce the capital costs involved in the manufacturing of nanocomposites with additional chemical and functionalization groups it is essential to evaluate the aspects of fibre bridging at simulation level. The computational modelling of the mechanical properties of graphene sheets and CNTs at atomic scale has been performed by several researchers using Finite Element techniques [1,2,5,6,31–34]. The Finite Element-based atomistic simulation techniques to represent general carbon nanostructures have been used for example by Scarpa et al. [1,7,8,31] and Pour et al. [2,35]. Scarpa and co-authors in particular have developed a multiscale hybrid atomistic FE technique to represent the interaction existing between C–C sp^2 and sp^3 bonds, van der Walls interactions [1,8,36], the influence of hydrogenated bonds [37], and recently extended the technique to simulate the mechanics of DNA strands [38]. Atomistic-FE methods have also been used to describe the nonlinear and fracture properties of graphene and carbon nanotubes [39,40], as well as the mechanical behaviour of nanocomposites and graphene reinforcements [6,41–43] Nanocomposites based on SLGS/SWCNT reinforcement can be considered as two-phase or multiphase materials, represented at their most basic configuration by the presence of a nanoinclusion

* Corresponding author.
E-mail address: S.Adhikari@swansea.ac.uk (S. Adhikari).

http://dx.doi.org/10.1016/j.compositesb.2016.06.070
1359-8368/

and a surrounding matrix. At meso and nanoscales the polymer matrix can be considered as a continuous structure. Using the hybrid atomistic-FE approach the SLGS/SWCNT nanoinclusions can be represented numerically by an array of hexagonally oriented beam elements (Bernoulli [44] or Timoshenko [31]), with their nodes being the carbon atoms. The polymer matrix at micro scale can be approximated by 3D solid tetrahedral elements (see Fig 1). The molecules of the polymer matrix are connected to carbon atoms through van der Waals forces represented by Lennard-Jones (LJ) potentials, when no functional groups are present. From the numerical standpoint, the LJ potential attractive and repulsive forces between the fibre and the matrix can be transferred through nonlinear spring elements [6,45].

This work aims at investigating the effects due to the presence of molecular inter-linkers between different combinations of nano fillers (SWCNT/SWCNT, SLGS/SLGS and SWCNT/SLGS – Fig. 2a–c respectively) on the overall pullout force and strength of the composite material. The hybridization of the fillers has been done, since such composites are multiphase in nature. Exploitation of such multiphase composite systems has become a major topic of interest in recent years [46–48]. The use of aliphatic diamines and aromatic phenylenediamine as connecting functional groups between single wall carbon nanotubes within a polyethylene matrix has been observed to produce a significant increase of the pullout tensile force and the energy dissipated at the interface between the matrix and the carbon nanotubes [49]. The present work explores further the concept by using a modified multiscale approach based on the atomistic – FE approach to produce Representative Volume Elements (RVEs) that describe the polymer matrix, nanomaterial reinforcements, chemical group interlinks and van der Walls interactions within a nonlinear materials, geometry and failure criteria modelling framework. In this work we will consider three different types of inter-linkers (Fig. 1): aliphatic diamines $(CH_2)_3N_2H_4$, long chain aliphatic diamines $(CH_2)_{10}N_2H_4$ and Phenylenediamine (referred to as PDA). In Fig. 1 the black atoms are referred to carbon, the blue atoms represent nitrogen, the white atoms are indicative of hydrogen, while the red atoms are representative of the connections between the polymer and the fillers. To the best of the Authors' knowledge, the work presented in this paper features two levels of novelty. The first is related to the multiscale model, that incorporates the simulation of chemical groups interconnecting matrix and the carbon nanostructures within an atomistic – FE method. The results of the proposed model are benchmarked against analogous data from open literature produced suing other molecular mechanics models. The second novelty lies within the prediction of the tensile pullout and shear strength of graphene/graphene and hybrid graphene/carbon nanotube reinforcements, and the assessment of the mechanical performance against interlinked SWCNT configurations already evaluated by other researchers. To the best of the Authors' knowledge these aspects have not been described in open literature so far.

2. Multiscale model of the nanocomposite structures

The sp^2 covalent bonds of the SWCNT and SLGS structures are represented here using deep shear Timoshenko with six degrees of freedom (3 translational and 3 rotational) beams [1,31]. The element type B31 from the ABAQUS element library has been used to simulate covalent bonds. The length of each beam is 0.142 nm (the equilibrium length of C–C sp^2) and the diameter (thickness) is 0.089 nm [31]. The equivalent mechanical properties of the beams representing the C–C bonds are calculated based on the energy equivalence between the beams' strain energy and the stoichiometric harmonic potential calculated through force constant methods [31]:

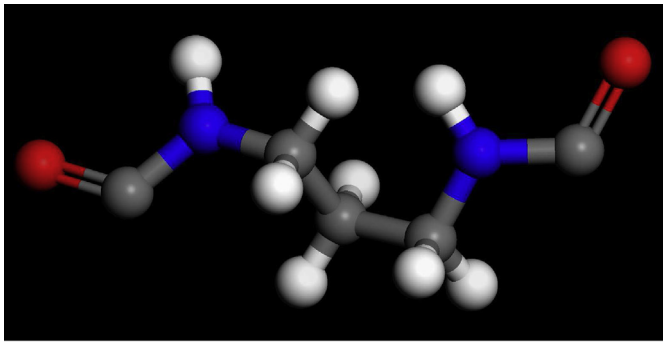

(a) Aliphatic diamine $(CH_2)_3N_2H_4$ (Inter-linker-1)

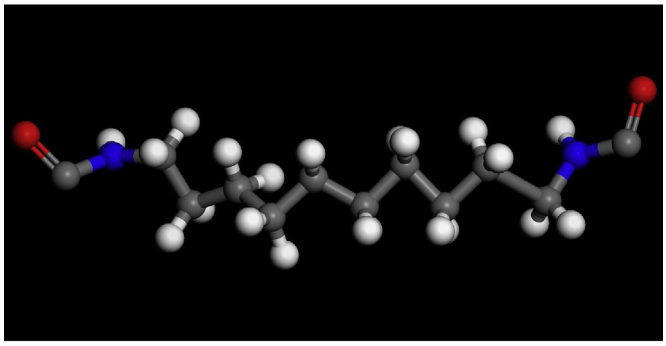

(b) Aliphatic diamine $(CH_2)_{10}N_2H_4$ (Inter-linker-2)

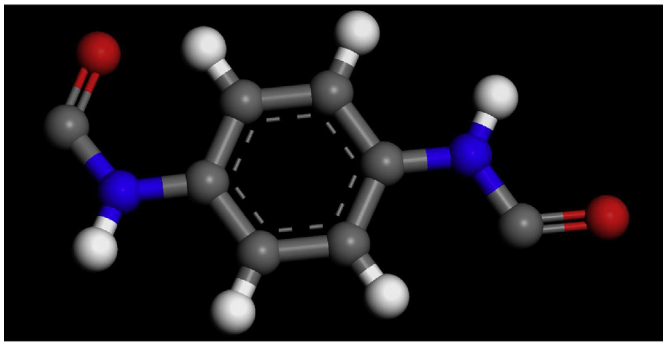

(c) Aromatic Phenylenediamine (PDA)

Fig. 1. Inter-linkers used to bridge fillers in nano-composite RVEs (From [49]).

$$\frac{k_r}{2}(\delta r)^2 = \frac{EA}{2L}(\delta r)^2 \tag{1}$$

$$\frac{k_\tau}{2}(\delta \phi)^2 = \frac{GJ}{2L}(\delta \phi)^2 \tag{2}$$

$$\frac{k_\theta}{2}(\delta \theta)^2 = \frac{EI}{2L}\frac{4+\Phi}{1+\Phi}(\delta \theta)^2 \tag{3}$$

in the above equations, k_r represents the stretching force constant and k_τ the out-of-plane torsional constant. The term k_θ represents a combined in-plane rotation (bending and torsion), consistent with the harmonic potential approach [31]. The term Φ is the shear correction factor, which becomes significant if the aspect ratio of beams is lower than 10 [50]. The numerical values of the constants mentioned in the above equations can be obtained by using the linearised Morse potential model [31] (k_r = 84.7 nN Å^{-1},

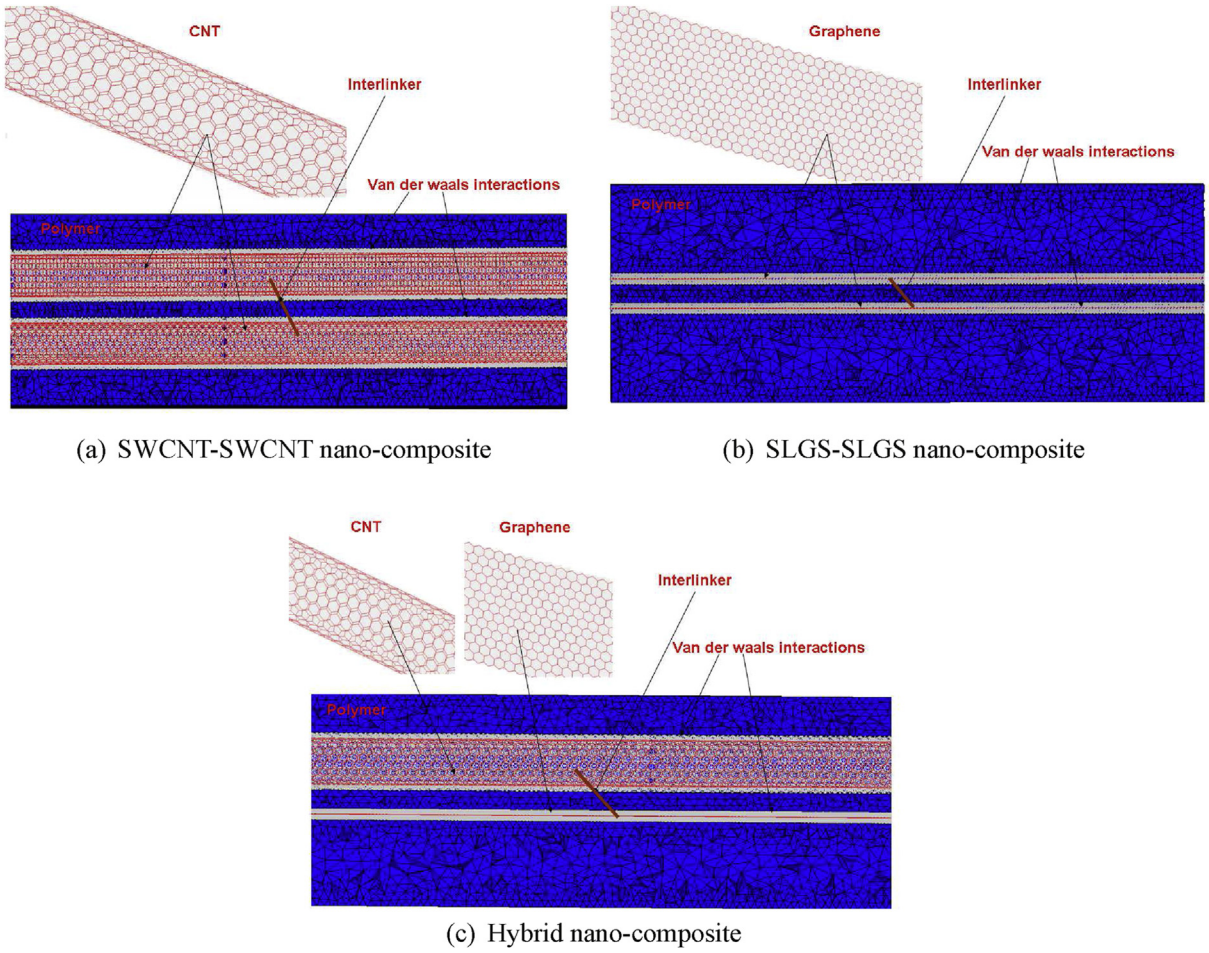

Fig. 2. Multiscale model of hybrid nano-composite with interlinkers: Three different types of inter-linkers have been simulated (refer Fig. 1).

Table 1
Element properties for the beam elements used to represent CC bonds. d stands for the diameter, l is the length, A is the cross sectional area, E represents the Young's modulus, ν is Poisson's ratio and φ is the shear correction factor [31].

Property	Value
d	0.089 nm
l	0.142 nm
A	1.01 nm^2
E	19.5 TPa
ν	0.23
φ	0.37

Table 2
Thicknesses, lengths and Young's moduli for bonds in inter-linkers [38].

Bond types	Bond length (Å)	Bond thickness (Å)	Young's modulus [TPa]
CH	1.08	1.01	6
CN	1.39	0.79	23.5
HN	1.01	0.8	16

$k_\theta = 9.00$ nN Å rad^{-2} and $k_\tau = 2.78$ nN Å rad^{-2}). For comprehensive understanding of this methodology, the readers are referred to [7,31,51]. The values of the equivalent material and the element property information for C–C bonds in SLGS and SWCNT are provided in Table 2.

In the present work the mechanical nonlinearity of the covalent bonds deformation has been ignored. The equivalent stress-strain curve for sp^2 C–C covalent bonds and graphene/carbon nanotubes can be found in various works [39,40,44,52,53]. The single C–C bond shows a linear regime under tensile loading up to 10% [40]. Armchair and zigzag graphene sheets in graphitic state show a substantial linearity of the tensile response also up to 10% in Molecular Dynamics models using AIREBO potential [54]. In a nano-composite with low loading (less than 0.5% wt fraction in the present work), one can also expect larger strain levels occurring in the polymer but not in the graphene sheet. Since the maximum tensile deformation in the present simulations corresponds to around 10% strain, the assumption of linear elastic regime with nonlinear geometric deformation for both SWCNT and SLGS can be considered justified. Similarly to the approach used for the C–C bonds, the mechanical properties of the other bonds in the interlinkers can also be obtained applying the same energy equivalence, this time using the Universal Force Field (UFF) model [38,55]. These equivalent mechanical properties are presented in Table 2. In order to simulate the tensile strength of interlinkers, a cutoff strain of about 20% has been assumed. If the bonds in the interlinkers are strained beyond this value, then the stiffness of the bonds will be reduced to zero. The 20% has been taken from the C–C bond inflection point of the curve present in Ref. [39]. However, during the simulation, the bonds in the interlinker do not get strained beyond 10%, due to contact with the polymer.

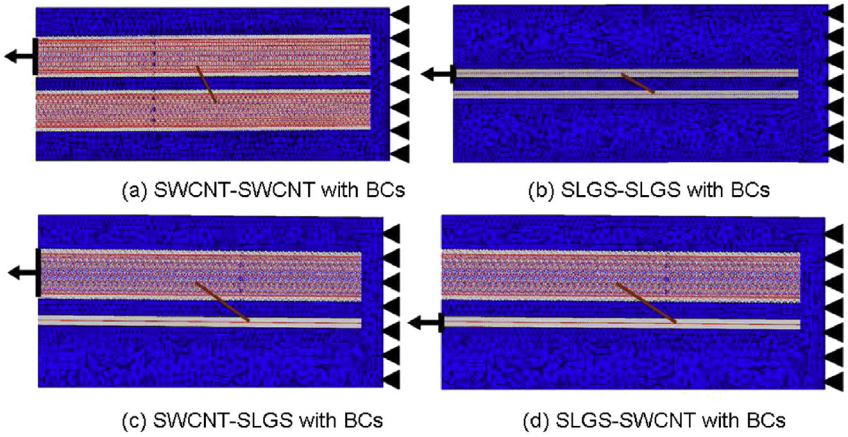

Fig. 3. Boundary conditions on four different multiscale FE models containing two fillers.

Table 3
Points of the stress-strain curve for epoxy matrix based on Ramberg Osgood approximation [58].

Stress in MPa	Strain in %
15	1.0
40	2.0
60	3.0
62	4.0

The graphene sheets are connected to the polymer matrix by van der Waals forces described by nonlinear springs providing attractive and repulsive forces and following the force-displacement model [1,8]:

$$F_{ij} = \frac{\partial V_{ij}}{\partial r} \tag{4}$$

where r is the atomic displacement along the **ij** connected carbon nanostructure/matrix atoms. The force between the atoms (ij) can also be represented by Ref. [56]:

$$F_{ij} = -12\,\varepsilon\left[\left(\frac{r_{min}}{y}\right)^{13} - \left(\frac{r_{min}}{y}\right)^{7}\right] \tag{5}$$

where $y = r_{min} + \delta r$, δr is the atomic displacement along the length **ij**. The r_{min} (in Å) is given by $2^{\frac{1}{6}}\,\sigma$, where $\sigma = (A/B)^{1/6}$. The terms B and A represent attractive and repulsive constants. For the carbon-polymer interaction we adopt the values given in Refs. [6,56,57], ($A = 3.4 \times 10^{-4}\,eV\times$ Å^{12} and $B = 5\times10^{-7}\,eV\times$ Å^{6}). The term ε is equal to $B^2/(4A)$. In the multiscale models we use nonlinear spring elements to simulate the interaction between reinforcement, with an equivalent force deflection curve calculated using Eq. (5). The type of element used in the ABAQUS solver is SPRINGA.

The polymer matrix has been discretized using 3D continuum elements with six degrees of freedom (C3D4 in ABAQUS). Isotropic material properties have been assumed to represent the material behaviour of an epoxy matrix (Young's modulus OF 2.0 GPa and Poisson's ratio of 0.3 [58]). The nonlinearity in the mechanical behaviour of the polymer matrix has been considered by using a Ramberg Osgood approximation [58]. Relevant points of the epoxy stress-strain curve are shown in Table 3. A damage criterion based on strain (5%) [43] has been assigned to ensure that the stiffness of the elements strained beyond that tensile threshold in the polymer becomes zero.

The dimensions of the RVEs are 60 Å × 40 Å× 110 Å. The SWCNTs used in this work are of armchair type (40,40) with a length of 98 Å. The SLGSs used consist also of an armchair type (40,40), again with a length of 98 Å. These dimensions ensure that both fillers have same surface area. As the SLGS offers a 2D surface, the contact interface with the polymer molecules occurs at both surfaces (top and bottom of the SLGS sheets). The force required to pull a fibre has been calculated by constraining one end of the nano-composite structure and applying a displacement to the end of filler in opposite side, similarly to the boundary conditions applied in Refs. [43,49]. One end of the RVE is constrained and a displacement is applied at the tab end of one of the nano-reinforcements (Fig. 3). The forces from one nanofiller are transferred to the other through the action of the inter-linker. The SWCNT-SWCNT nanocomposite contains two SWCNTs as reinforcements, with one of them being the primary filler (the one to which the end deformation is applied). A similar topology is applied to the SLGS-SLGS model. The SLGS-SWCNT model has the single layer graphene sheet at the reinforcement subjected to the external displacement. The pullout force is calculated as the reaction force measured at the end of the entire RVE where the displacement has been applied to the primary reinforcement. A node-to-element contact definition has been assigned between the nodes of the filler, inter-linkers and the surface of 3D elements in the polymer matrix. A nonlinear Newton-Raphson solver with switch on large deformation effects has been used to simulate the fibre pullout [59]. The simulation is executed until the reinforcement comes out of the matrix at a distance of 14.5 Å. Beyond this cut-off length the elements of the reinforcement and the spring elements representing the LJ potential have been found to be unstable. During the simulation it was essential to deactivate the interface bonds between the filler and matrix if the deflection developed is higher than the cut-off distance of 0.85 nm [6]. It was also necessary to generate new bonds if a displaced carbon atom comes in contact with another atom of the matrix. Within the FE code ABAQUS^{TM} version 6.10, this operation is performed by using the commands *Restart and *Modelchange [59]. The nodal displacements in the spring elements (interface bonds) are recorded at each increment step of the nonlinear loading. If the nodal displacement is found to be beyond the cut-off distance the analysis is stopped and restarted with an updated position of the nodes belonging to the spring elements. Another *Restart command is then issued to restart the run from the same increment. Activation and de-activation of the spring element sets are performed using the commands *Modelchange, Remove and *Modelchange, Add.

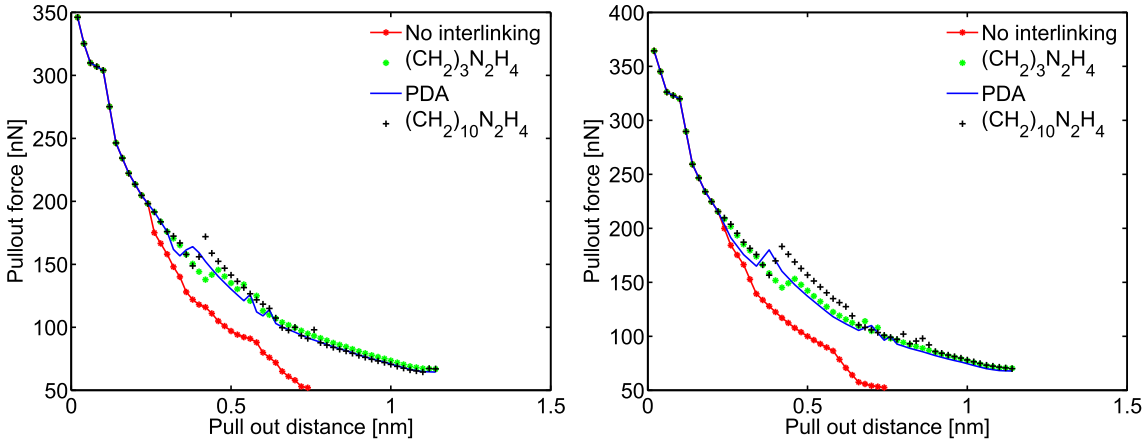

(a) SWCNT-SWCNT (b) SLGS-SLGS

Fig. 4. Force required to pull out the fibre from the SLGS-SLGS and SWCNT-SWCNT nanocomposites.

This process has been referred to as the "debonding" and "rebonding" mechanism in the current work. Possible interlocking phenomenon due to the interaction between the carbon nano-reinforcements and matrix are taken into by defining a contact interaction (node to surface) between the fillers and polymer. Similar multiscale models have been developed in Ref. [45] and been used in Ref. [41]. However, these models do not describe the presence of interlinks between the nanoinclusion and the matrix as discrete functional groups.

3. Results and discussions

The pullout forces versus the tensile deformation are shown for various types of nano-reinforcement and inter-linkers in Figs. 4 and 5. The general trend of these forces is very similar for all the four boundary conditions considered, and this indicates that the two types of nano-reinforcement are quite close in terms of mechanical behaviour under the conditions assumed in this work. It is however possible to observe some differences in terms of magnitudes of the pullout forces when the reinforcements are directly compared one against the other. The maximum pullout force observed for a composite with a SLGS being the primary reinforcement is 370 nN, 6% higher compared to the case in which the single wall carbon nanotube is the primary filler (refer to Fig. 4(a)). The higher interfacial strength in the SLGS nanocomposite due to the higher contact surface area between the reinforcement and the polymer is believed to be responsible for this behaviour. The same trend has been also observed in the other two nanocomposite topologies (Fig. 5(a) and (b)) because the primary reinforcements in the SWCNT/SLGS and SLGS/SWCNT configurations are the same as the ones in the SLGS/SLGS and SWCNT/SWCNT nanocomposites respectively (Fig. 3). The force/displacements curves remain almost identical up to a pullout distance of 0.2 nm, because only the primary reinforcement is bearing the load at this stage. After this threshold distance a sudden increase in load (first peak) can be observed due to the debonding and rebonding of the van der Walls interactions in the primary reinforcement. Beyond the 0.2 nm pullout distance the curves however diverge because the load starts to be shared by the inter-linker groups. The composites without inter-linkers generate lower reaction forces beyond this distance. In the case of the nanocomposites with the inter-linkers a sudden increase in load can be observed, with its magnitude depending upon the type of inter-linker used. The model with the $(CH_2)_{10}N_2H_4$ groups generates the highest load at this point, because of its higher length that allows to transfer the load at higher tensile displacements. The PDA inter-linker also offers an

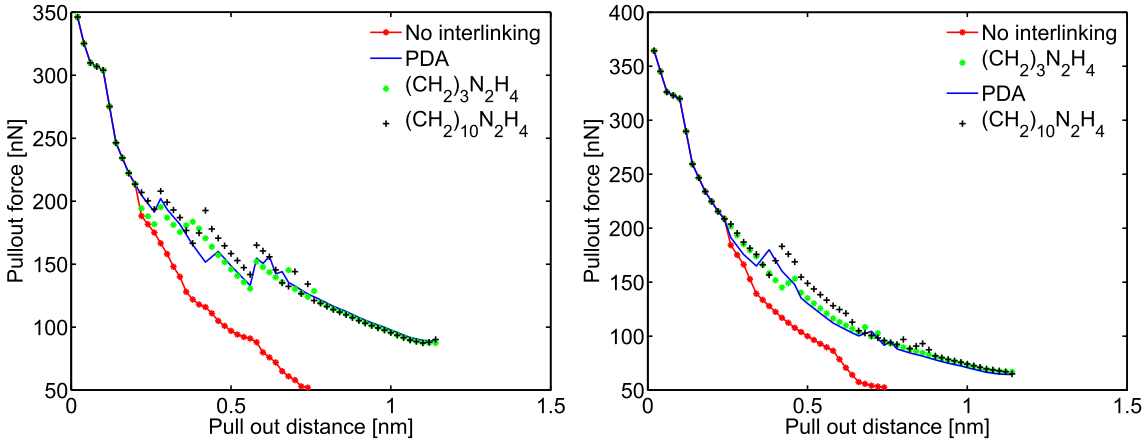

(a) Hybrid SWCNT-SLGS composite (b) Hybrid SLGS-SWCNT composite

Fig. 5. Force required to pull out the fibre from the hybrid nanocomposites.

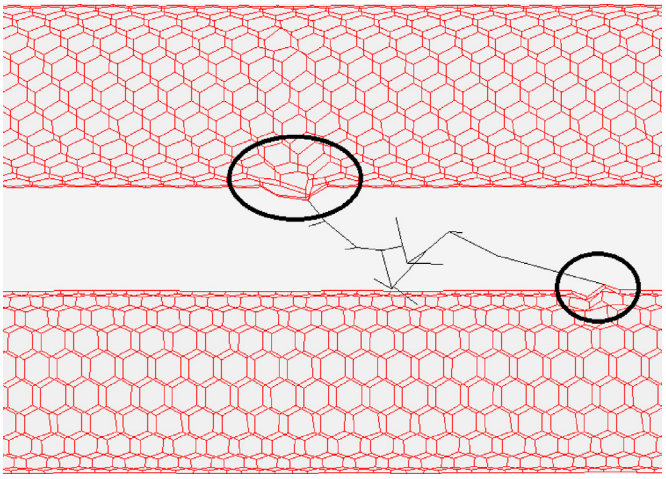

Fig. 6. Evidence of localised auxetic effect between the SWCNT reinforcements provided by the inter-linker effect.

increase in terms of load to pullout, since it possess a larger surface that facilitates the contact with the surrounding polymer. After the threshold distance the load will be distributed uniformly in the two reinforcements. As the load is transferred to the couple of reinforcements through the inter-linkers the walls of the carbon nanostructures distort, leading to interlocking of these walls with the surrounding polymer. Such wall distortion in the case of the SWCNT fillers can be considered a localised auxetic effect [49] (Fig. 6), similarly to what observed in auxetic polymeric fibres subjected to pullout tests [60]. As also demonstrated by MD simulations carried previously by some of the Authors [49], the auxetic effect enhances the pullout resistance of the nano reinforcements because of the fretting of the nanofiller against the matrix system due to the transverse tensile expansion (negative Poisson's ratio effect), leading to increased toughness and energy dissipation of the overall structure [61]. Further discontinuities in the load/displacement curves can be observed around 0.75 nm as a result of the debonding/rebonding occurring within the secondary reinforcement. The reaction force generated by the secondary filler in the SWCNT-SWCNT nanocomposite is around 160 nN, 12.5% lower than in the case of the SLGS/SLGS configuration, and a further indication that the single layer graphene offers an enhanced uniaxial tensile mechanical performance, also a secondary reinforcements. Similar trends can also be noticed in the hybrid SWCNT/SLGS and SLGS/SWCNT nanocomposites.

The interfacial strength between the filler and the matrix can be calculated as [49]:

$$E_{pullout} = 2\pi rL\tau_i d - \pi r\tau_i d^2 \quad (6)$$

in the above equation, τ_i is the interfacial shear strength, r and L are the width and length of the reinforcements, x is the axial location in which the strength of the nanocomposite is measured and d is the deformation of the nanoreinforcement. The pullout energy in kcal/mol can be calculated by $F_{pullout} = \frac{\partial E_{pullout}}{\partial d}$, in which $F_{pullout}$ is the lowest pullout force (in nN) measured during the simulation and d is deformation expressed in nm. The interfacial strength τ_i measured in the current work and compared with the one determined by other authors is given in Table 4.

The magnitude of the interfacial strength computed in the present work is within the lower end of the reported values in open literature (44 MPa − 102 MPa). There is a noticeable scatter in the values of the interfacial shear strength, the variability attributed to the different types of force models adopted in the molecular dynamics simulations, the nature of the polymer matrix and the nanoreinforcement used. The highest interfacial strength value we have observed in open literature is 500 MPa [62]. Gou et al. [63] have also simulated the presence of a SWCNT reinforcement in an epoxy matrix and reported 75 MPa as the interfacial strength, 75% higher than what has been simulated in the present work with no use of inter-linker. The maximum interfacial strength recorded in the present work is 102.32 MPa (obtained by interlinking SLGS fibres with PDA). This value is very close to that of conventional/commercial carbon fibre composites [74–78]. It is also worth noticing that in the case of stick-slip damping provided by single wall carbon nanotubes embedded in epoxy matrix, the values of the interfacial shear strength used to fit experimental modal loss

Table 4
Interfacial strength reported in open literature and present work. The values of present work are from SWCNT-SWCNT and SLGS-SLGS nano-composites only. The terms PEEK, MWCNT and rGO in the table refers to Polyether ether ketone, multiwalled carbon nano tubes and reduced graphene oxide respectively.

Authors	Filler type	Interfacial strength (MPa)	Inter-linker type	Matrix type	Analysis type
Wagner et al. [62]	MWCNT	500	–	Urethane based	Experimental
Gou et al. [63]	SWCNT	75.00	–	Epoxy	MD
Liao and Li [64]	SWCNT	160.00	–	Polystyrene	MD
Rahman and Haque [65]	SLGS	88.00	–	Epoxy	MD
Lv et al. [66]	FSLGS	70.00	–	Polyethylene	MD
Chowdhury and Okabe [67]	SWCNT	75.00	–	Epoxy	MD
Barber et al. [68]	MWCNT	47.00	–	Polyethylene	Experimental
Sager et al. [69]	MWCNT	86.6	–	T650 carbon-Epoxy	KellyTyson model [70]
Jang et al. [71]	rGO	136.6	–	Polycarbonate	Semi-Empirical
Tsuda et al. [72]	MWCNT	14	–	PEEK	Experimental
Roy et al. [73]	SWCNT	160	–	Polyvinylalcohol	Experimental
Present work	SLGS	49.26	–	Epoxy	Atomistic
Present work	SLGS	62.14	PDA	Epoxy	Atomistic
Present work	SLGS	95.25	$(CH_2)_3N_2H_4$	Epoxy	Atomistic
Present work	SLGS	102.32	$(CH_2)_{10}N_2H_4$	Epoxy	Atomistic
Present work	SWCNT	44.28	–	Epoxy	Atomistic
Present work	SWCNT	58.25	PDA	Epoxy	Atomistic
Present work	SWCNT	88.42	$(CH_2)_3N_2H_4$	Epoxy	Atomistic
Present work	SWCNT	98.13	$(CH_2)_{10}N_2H_4$	Epoxy	Atomistic
Zhang et al. [49]	SWCNT	46.48	–	Polyethylene	MD
Zhang et al. [49]	SWCNT	63.45	PDA	Polyethylene	MD
Zhang et al. [49]	SWCNT	90.26	$(CH_2)_3N_2H_4$	Polyethylene	MD
Zhang et al. [49]	SWCNT	100.85	$(CH_2)_{10}N_2H_4$	Polyethylene	MD

factors values varies as low as 0.2 MPa – 2 MPa [79]. In the current work, the interfacial strength computed for the SWCNT-SWCNT type nanocomposites is very close to that computed with MD in Ref. [49] with similar inter-linkers and polyethylene matrix. The maximum difference is found be around 2% (for the inter-linker ($(CH_2)_{10}N_2H_4$)). In the cases of both SWCNT/SWCNT and SLGS/SLGS nanocomposites the configuration with the ($(CH_2)_{10}N_2H_4$) inter-linker offers the hights interfacial shear strength efficiency, while the ($(CH_2)_3N_2H_4$) group provides the weakest contribution due to its short length, leading to an overall lower stiffness.

4. Conclusion

The pullout and interfacial strengths in nanocomposites with hybrid inter-linker reinforcements have been predicted using a numerical nonlinear tensile atomistic-FE multiscale model. The model predicts a localised geometric distortion when the nano-reinforcements interact with the matrix because of the presence of an inter-linked (auxetic effect), as also predicted in previous works using molecular dynamics simulations. The bridging of the nano-reinforcements with a link molecule enhances the pullout strength by upto 30%. The stiffness and surface area of the inter-linkers play a role in enhancing the mechanical strength of overall nano-composites, with the $(CH_2)_{10}N_2H_4$ interlinker found to be the most in transferring the load. The composites with SWCNT acting both as primary and secondary reinforcements show a slight enhanced pullout performance (2% more) than the graphene layer based and hybrid nanoreinforcements. As a secondary filler the SWCNTs also offer 10% extra pullout strength when compared to single layer graphene sheets. The interfacial shear strength between the nanoreinforcements and the matrix computed with the multiscale technique shows a very good agreement with analogous configurations simulated using Molecular Dynamics, and also shows a correlation between the specific carbon nanostructure used and the chemical groups used for the inter-link. The model presented in this paper and the configurations of inter-linked nanocomposites proposed may be used to further the. The novelty of this research lies in the development of a simulation methodology that can predict the behaviour of multiphase nanocomposites at multiple length scales in which the nanofillers are bridged by interlinkers.

Acknowledgements

SA acknowledges the Royal Society for the Wolfson Research Merit Award. FS thanks the support of the FP7-NMP-2010-LA-2010-246067 M-RECT project for the logistics support.

References

[1] Chandra Y, Chowdhury R, Scarpa F, Adhikari S. Vibrational characteristics of bilayer graphene sheets. Thin Solid Films 2011;519(18):6026–32.
[2] Sakhaee-Pour A, Ahmadian M, Naghdabadi R. Vibrational analysis of single-layered graphene sheets. Nanotechnology 2008;19(8):085702.
[3] Chowdhury R, Adhikari S, Scarpa F, Friswell M. Transverse vibration of single-layer graphene sheets. J Phys D Appl Phys 2011;44(20):205401.
[4] Gupta S, Batra R. Elastic properties and frequencies of free vibrations of single-layer graphene sheets. J Comput Theor Nanosci 2010;7(10):2151–64.
[5] Tserpes K, Papanikos P. Finite element modeling of single-walled carbon nanotubes. Compos Part B Eng 2005;36(5):468–77.
[6] Shokrieh MM, Rafiee R. Prediction of young's modulus of graphene sheets and carbon nanotubes using nanoscale continuum mechanics approach. Mater Des 2010;31(2):790–5.
[7] Scarpa F, Adhikari S. A mechanical equivalence for poisson's ratio and thickness of c–c bonds in single wall carbon nanotubes. J Phys D Appl Phys 2008;41(8):085306.
[8] Scarpa F, Adhikari S, Gil A, Remillat C. The bending of single layer graphene sheets: the lattice versus continuum approach. Nanotechnology 2010;21(12):125702.
[9] Sadeghi M, Naghdabadi R. Nonlinear vibrational analysis of single-layer graphene sheets. Nanotechnology 2010;21(10):105705.
[10] Yu M-F, Files BS, Arepalli S, Ruoff RS. Tensile loading of ropes of single wall carbon nanotubes and their mechanical properties. Phys Rev Lett 2000;84(24):5552.
[11] Novoselov KS, Geim AK, Morozov S, Jiang D, Zhang Y, Dubonos S, et al. Electric field effect in atomically thin carbon films. Science 2004;306(5696):666–9.
[12] Chowdhury R, Adhikari S, Rees P. Zigzag graphene nanoribbon single-electron transistors. Phys B Condens Matter 2012;407(5):855–8.
[13] Liang J, Xu Y, Huang Y, Zhang L, Wang Y, Ma Y, et al. Infrared-triggered actuators from graphene-based nanocomposites. J Phys Chem C 2009;113(22):9921–7.
[14] Zhang H-B, Zheng W-G, Yan Q, Yang Y, Wang J-W, Lu Z-H, et al. Electrically conductive polyethylene terephthalate/graphene nanocomposites prepared by melt compounding. Polymer 2010;51(5):1191–6.
[15] Dimitrakopoulos C, Lin Y-M, Grill A, Farmer DB, Freitag M, Sun Y, et al. Wafer-scale epitaxial graphene growth on the si-face of hexagonal sic (0001) for high frequency transistors. J Vac Sci Technol B 2010;28(5):985–92.
[16] Lin Y-M, Dimitrakopoulos C, Jenkins KA, Farmer DB, Chiu H-Y, Grill A, et al. 100-ghz transistors from wafer-scale epitaxial graphene. Science 2010;327(5966):662.
[17] Liu Y, Kumar S. Polymer/carbon nanotube nano composite fibers review. ACS Appl Mater Interfaces 2014;6(9):6069–87.
[18] Murmu T, Adhikari S. Nonlocal frequency analysis of nanoscale biosensors. Sensors Actuators A Phys 2012;173(1):41–8.
[19] Andrews R, Weisenberger M. Carbon nanotube polymer composites. Curr Opin Solid State Mater Sci 2004;8(1):31–7.
[20] Adhikari S, Chowdhury R. Zeptogram sensing from gigahertz vibration: graphene based nanosensor. Phys E Low-dimensional Syst Nanostruct 2012;44(7–8):1528–34.
[21] Du J, Cheng H-M. The fabrication, properties, and uses of graphene/polymer composites. Macromol Chem Phys 2012;213(10–11):1060–77.
[22] D'Aloia A, Marra F, Tamburrano A, De Bellis G, Sarto M. Electromagnetic absorbing properties of graphene–polymer composite shields. Carbon 2014;73:175–84.
[23] Karlicic D, Kozic P, Adhikari S, Cajic M, Murmu T, Lazarevic M. Nonlocal biosensor based on the damped vibration of single-layer graphene influenced by in-plane magnetic field. Int J Mech Sci 2015;96–97(6):132–42.
[24] Adhikari S, Murmu T. Nonlocal mass nanosensors based on vibrating monolayer graphene sheets. Sensors Actuators B Chem 2013;188(11):1319–27.
[25] Stankovich S, Dikin DA, Dommett GH, Kohlhaas KM, Zimney EJ, Stach EA, et al. Graphene-based composite materials. Nature 2006;442(7100):282–6.
[26] Wajid AS, Das S, Irin F, Ahmed H, Shelburne JL, Parviz D, et al. Polymer-stabilized graphene dispersions at high concentrations in organic solvents for composite production. Carbon 2012;50(2):526–34.
[27] Chen W, Tao X. Production and characterization of polymer nanocomposite with aligned single wall carbon nanotubes. Appl Surf Sci 2006;252(10):3547–52.
[28] Satyanarayana N, Rajan KS, Sinha SK, Shen L. Carbon nanotube reinforced polyimide thin-film for high wear durability. Tribol Lett 2007;27(2):181–8.
[29] Hussain F, Hojjati M, Okamoto M, Gorga RE. Review article: polymer-matrix nanocomposites, processing, manufacturing, and application: an overview. J Compos Mater 2006;40(17):1511–75.
[30] Zhang J, Jiang D. Interconnected multi-walled carbon nanotubes reinforced polymer-matrix composites. Compos Sci Technol 2011;71(4):466–70.
[31] Scarpa F, Adhikari S, Phani AS. Effective elastic mechanical properties of single layer graphene sheets. Nanotechnology 2009;20(6):065709.
[32] Shokrieh MM, Rafiee R. On the tensile behavior of an embedded carbon nanotube in polymer matrix with non-bonded interphase region. Compos Struct 2010;92(3):647–52.
[33] Saavedra Flores EI, Adhikari S, Friswell MI, Scarpa F. Hyperelastic axial buckling of single wall carbon nanotubes. Phys E Low-dimensional Syst Nanostruct 2011;44(2):525–9.
[34] Saavedra Flores EI, Adhikari S, Friswell MI, Scarpa F. Hyperelastic finite element model for single wall carbon nanotubes in tension. Comput Mater Sci 2011;50(3):1083–7.
[35] Sakhaee-Pour A. Elastic buckling of single-layered graphene sheet. Comput Mater Sci 2009;45(2):266–70.
[36] Liu X, Metcalf TH, Robinson JT, Houston BH, Scarpa F. Shear modulus of monolayer graphene prepared by chemical vapor deposition. Nano Lett 2012;12(2):1013–7. pMID: 22214257.
[37] Scarpa F, Chowdhury R, Adhikari S. Thickness and in-plane elasticity of graphane. Phys Lett A 2011;375(20):2071–4.
[38] Adhikari S, Saavedra Flores EI, Scarpa F, Chowdhury R, Friswell MI. A hybrid atomistic approach for the mechanics of deoxyribonucleic acid molecules. ASME J Nanotechnol Eng Med 2013;4(4). 041006:1–7.
[39] Baykasoglu C, Mugan A. Nonlinear fracture analysis of single-layer graphene sheets. Eng Fract Mech 2012;96:241–50.
[40] Baykasoglu C, Mugan A. Coupled molecular/continuum mechanical modeling of graphene sheets. Phys E Low-dimensional Syst Nanostruct 2012;45:151–61.
[41] Shokrieh MM, Rafiee R. Development of a full range multi-scale model to obtain elastic properties of cnt/polymer composites. Iran Polym J 2012;21(6):397–402.
[42] Shokrieh MM, Rafiee R. Stochastic multi-scale modeling of cnt/polymer composites. Comput Mater Sci 2010;50(2):437–46.
[43] Chandra Y, Scarpa F, Chowdhury R, Adhikari S, Sienz J. Multiscale hybrid

atomistic-fe approach for the nonlinear tensile behaviour of graphene nanocomposites. Compos Part A Appl Sci Manuf 2013;46:147–53.
[44] Tserpes K, Papanikos P, Tsirkas S. A progressive fracture model for carbon nanotubes. Compos Part B Eng 2006;37(7):662–9.
[45] Li C, Chou T-W. A structural mechanics approach for the analysis of carbon nanotubes. Int J Solids Struct 2003;40(10):2487–99.
[46] Gupta TK, Singh BP, Mathur RB, Dhakate SR. Multi-walled carbon nanotube–graphene–polyaniline multiphase nanocomposite with superior electromagnetic shielding effectiveness. Nanoscale 2014;6(2):842–51.
[47] Gouda PS, Kulkarni R, Kurbet S, Jawali D. Effects of multi walled carbon nanotubes and graphene on the mechanical properties of hybrid polymer composites. Adv Mater Lett 2013;4(4):261–70.
[48] Araby S, Saber N, Ma X, Kawashima N, Kang H, Shen H, et al. Implication of multi-walled carbon nanotubes on polymer/graphene composites. Mater Des 2015;65:690–9.
[49] Zhang J, Jiang D, Scarpa F, Peng H-X. Enhancement of pullout energy in a single-walled carbon nanotube-polyethylene composite system via auxetic effect. Compos Part A Appl Sci Manuf 2013;55(0):188–94.
[50] Timoshenko S, Woinowsky-Krieger S, Woinowsky-Krieger S. Theory of plates and shells, 2. New York: McGraw-hill; 1959.
[51] Scarpa F, Adhikari S, Chowdhury R. The transverse elasticity of bilayer graphene. Phys Lett A 2010;374(19):2053–7.
[52] Georgantzinos S, Giannopoulos G, Anifantis N. Investigation of stress–strain behavior of single walled carbon nanotube/rubber composites by a multiscale finite element method. Theor Appl Fract Mech 2009;52(3):158–64.
[53] Mohammadpour E, Awang M. Nonlinear finite-element modeling of graphene and single-and multi-walled carbon nanotubes under axial tension. Appl Phys A 2012;106(3):581–8.
[54] Pei Q, Zhang Y, Shenoy V. A molecular dynamics study of the mechanical properties of hydrogen functionalized graphene. Carbon 2010;48(3):898–904.
[55] Rappé AK, Casewit CJ, Colwell K, Goddard Iii W, Skiff W. Uff, a full periodic table force field for molecular mechanics and molecular dynamics simulations. J Am Chem Soc 1992;114(25):10024–35.
[56] Girifalco L, Hodak M, Lee RS. Carbon nanotubes, buckyballs, ropes, and a universal graphitic potential. Phys Rev B 2000;62(19):13104.
[57] Battezzati L, Pisani C, Ricca F. Equilibrium conformation and surface motion of hydrocarbon molecules physisorbed on graphite. J Chem Soc Faraday Trans 2 Mol Chem Phys 1975;71:1629–39.
[58] Yarrington P, Zhang J, Collier C, Bednarcyk BA. Failure analysis of adhesively bonded composite joints. In: 46 th AIAA/ASME/ASCE/AHS/ASC structures, structural dynamics & materials conference; 2005.
[59] ABAQUS. ABAQUS documentation and manual version 6.10. Simulia Inc.: Dassault Systèmes; 2012.
[60] Simkins V, Alderson A, Davies P, Alderson K. Single fibre pullout tests on 513 single fibre pullout tests on auxetic polymeric fibres. J Mater Sci 2005;40(16):4355–64.
[61] Bianchi M, Scarpa F, Smith C. Stiffness and energy dissipation in polyurethane auxetic foams. J Mater Sci 2008;43(17):5851–60.
[62] Wagner H, Lourie O, Feldman Y, Tenne R. Stress-induced fragmentation of multiwall carbon nanotubes in a polymer matrix. Appl Phys Lett 1998;72(2):188–90.
[63] Gou J, Minaie B, Wang B, Liang Z, Zhang C. Computational and experimental study of interfacial bonding of single-walled nanotube reinforced composites. Comput Mater Sci 2004;31(3):225–36.
[64] Liao K, Li S. Interfacial characteristics of a carbon nanotube–polystyrene composite system. Appl Phys Lett 2001;79(25):4225–7.
[65] Rahman R, Haque A. Molecular modeling of crosslinked graphene–epoxy nanocomposites for characterization of elastic constants and interfacial properties. Compos Part B Eng 2013;54:353–64.
[66] Lv C, Xue Q, Xia D, Ma M, Xie J, Chen H. Effect of chemisorption on the interfacial bonding characteristics of graphene- polymer composites. J Phys Chem C 2010;114(14):6588–94.
[67] Chowdhury S, Okabe T. Computer simulation of carbon nanotube pull-out from polymer by the molecular dynamics method. Compos Part A Appl Sci Manuf 2007;38(3):747–54.
[68] Barber AH, Cohen SR, Wagner HD. Measurement of carbon nanotube–polymer interfacial strength. Appl Phys Lett 2003;82(23):4140–2.
[69] Sager R, Klein P, Lagoudas D, Zhang Q, Liu J, Dai L, et al. Effect of carbon nanotubes on the interfacial shear strength of t650 carbon fiber in an epoxy matrix. Compos Sci Technol 2009;69(7):898–904.
[70] Kelly A, Tyson WR. Tensile properties of fibre-reinforced metals: copper/tungsten and copper/molybdenum. J Mech Phys Solids 1965;13(6):329–50.
[71] Jang H-K, Kim H-I, Dodge T, Sun P, Zhu H, Nam J-D, et al. Interfacial shear strength of reduced graphene oxide polymer composites. Carbon 2014;77:390–7.
[72] Tsuda T, Ogasawara T, Deng F, Takeda N. Direct measurements of interfacial shear strength of multi-walled carbon nanotube/peek composite using a nano-pullout method. Compos Sci Technol 2011;71(10):1295–300.
[73] Roy D, Bhattacharyya S, Rachamim A, Plati A, Saboungi M-L. Measurement of interfacial shear strength in single wall carbon nanotubes reinforced composite using raman spectroscopy. J Appl Phys 2010;107(4):043501.
[74] Ho H, Drzal T. Interfacial shear strength. In: Tenth international conference on composite materials. IV. Characterization and ceramic matrix composites; 1995. p. 203–9.
[75] Yusong Y, Zhao Y, Li Y, Dong Q, Chen D. Effect of sizing on the interfacial shear strength of carbon fiber/epoxy resin monofilament composite. J Wuhan Univ Technol. Mater Sci. Ed 2014;29(3):483–7.
[76] Deng S, Ye L, Mai Y-W. Measurement of interfacial shear strength of carbon fibre/epoxy composites using a single fibre pull-out test. Adv Compos Mater 1998;7(2):169–82.
[77] Nightingale C, Day R. Flexural and interlaminar shear strength properties of carbon fibre/epoxy composites cured thermally and with microwave radiation. Compos Part A Appl Sci Manuf 2002;33(7):1021–30.
[78] Carbon fibre composite data sheet (M55 J UD). New Jersey, USA: Torray Corporation; 2014.
[79] Zhou X, Shin E, Wang K, Bakis CE. Interfacial damping characteristics of carbon nanotube-based composites. Compos Sci Technol 2004;64:2425.